PROCESSING AND MICROSTRUCTURE OF WC-CO CERMETS BY LASER ENGINEERED NET SHAPING

Y. Xiong[*], J. E. Smugeresky[+], E. J. Lavernia[*], J. M. Schoenung[*]
[*]Department of Chemical Engineering and Materials Science; University of California; Davis, CA 95616
[+]Sandia National Laboratories; Livermore, CA 94551

Abstract

Submicron-sized tungsten carbide-cobalt (WC-Co) powder and nanostructured WC-Co powder were applied to make thick wall samples by the Laser Engineered Net Shaping (LENS[®]) process. It was found that decomposition and decarburization of WC was limited during laser deposition because of the features of the LENS[®] process: high cooling rate, short heating time, and low oxygen concentration. The effects of working distance, as well as laser power, powder feed rate, and traverse speed on microstructure were studied in this paper. Thermal behavior leading to the observed microstructures that result from the variations in the processing parameters was investigated in detail.

Introduction

Cemented carbides, like WC-Co, have been widely used as cutting tools, dies, rock drills, wear-resistant nozzles and coatings for several decades. These applications result from the unique combination of high hardness and toughness of the WC-Co cermet. Currently, there are a number of techniques to synthesize WC-Co cermet bulk and coating materials. These include conventional powder metallurgy processes followed by liquid phase sintering (LPS) and machining (subsequently referred to as "the P/M process") [1-3], thermochemical techniques [4, 5], spark plasma sintering (SPS) [6, 7], vacuum plasma spraying [8] and high velocity oxy-fuel (HVOF) spraying [9, 10]. The P/M process is the most common method used for bulk WC-Co manufacturing. However, decomposition and decarburization of WC into brittle phases, such as W_2C and $Co_xW_yC_z$ compounds are difficult to avoid unless extra free carbon is applied. Further research has indicated that with fine powders, abnormal growth of WC particles will occur during sintering, which will affect the mechanical properties. The Laser Engineered Net Shaping (LENS[®]) technology is an extension of rapid prototyping (RP) technologies into the direct fabrication of alloy parts [11]. The most significant features of the LENS[®] technology are its high cooling/solidification rate, rapid prototyping capability, and proper shape control. Thus, this technology has advantages to control grain growth, increase process efficiency and save machining costs. It has been used to fabricate a broad range of materials, including stainless steels, nickel-based superalloys, copper alloys, titanium alloys and functional composites with improved physical and mechanical material properties [11-14]. To explore the application of the LENS[®] technology, an understanding of the relationship between process conditions and sample profile and microstructure is of special interest. However, reports on this topic are limited to the effects of laser power and traverse speed [12, 15, 16]. Furthermore, research in the application of the LENS[®] process to the fabrication of WC-Co cermets is also limited.

In this work, the LENS[®] process was used to make WC-Co thick wall samples. A comprehensive analysis of the effects of process conditions, including laser power, powder feed rate, traverse speed, and working distance, was investigated.

Experimental Methods

A. Feedstock Powders

Two feedstock powders were used in this work. The first was a submicron-sized WC-13 wt.% Co powder (powder A), produced via a wet-chemical plus spray-drying process, provided by Inframat Corp. Farmington, CT. The powder has a granule size ranging from 40 μm to 110 μm. The second powder was a nanocrystalline WC-10 wt.% Co powder (powder B), made by MBN Nanomaterialia S.p.A. in Vascon di Carbonera, Italy with a granule size range of 45 μm to 90 μm. The nanocrystalline WC-10 wt.% Co powder was produced by high-energy ball milling. The descriptors of "submicron" and "nanocrystalline" refer to the size of the WC particles within the cermet granules.

B. Process Description

A LENS® 750 system (OPTOMEC, Albuquerque, NM) was used to deposit WC-Co thick wall samples. The LENS® process is operated in a sealed chamber filled with argon gas [17]. A 750 W CW Nd: YAG laser is applied to create a molten pool on a metal substrate. During this process, powder is delivered in a gas stream of argon, through nozzles, into the molten pool. The laser and nozzles remain stationary while the substrate is moved, providing a controlled deposition of a thin line (a thin layer of finite width and height on the order of 0.1 mm). The part shape is controlled through a pre-programmed CAD model. The process parameters that were investigated include laser power, traverse speed, powder feed rate and working distance (the spacing between the powder delivery nozzles and the plane on which powders are deposited). The applied value ranges for these parameters are listed in Table 1. The oxygen concentration was controlled at less than 5 ppm. The CAD solid model had the shape of a thick wall (1.5 mm in thickness with multiple parallel lines for each layer).

Table 1. Applied value ranges for process parameters during the LENS® process.

Experimental Parameter	Range
Laser power	140-200 W
Powder feed rate	7-21 g/min
Traverse speed	2-11 mm/s
Working plane	Focal plane ± 4 mm

*: g/min stands for grams per minute

C. Property Characterization

The composition of the as-received powders was analyzed by Luvak Inc. (Boylston, MA, USA) using standard ASTM E 1097-03 and 1019-03 procedures. The phase characterization of the as-received powders and the thick wall specimens were conducted by X-ray diffraction (XRD) using a Scintag XDS 2000 diffractometer operated at 40 kV with Cu Kα (λ= 0.15406 nm) radiation. The microstructure for the two types of powder and the thick wall specimens was analyzed with a PHILIPS FEI XL 30 SFEG Scanning Electron Microscope (SEM). Energy dispersive X-ray spectroscopy (EDS) was also used with SEM to distinguish different phases. The density of the thick wall specimens was tested by an AG204 balance made by Mettler-Toledo (Schweiz) GmbH with standard procedures for the determination of solid density.

Results and Discussion

A. Microstructure of Powder A and B

The SEM images in Figs. 1 (a) and (b) reveal the morphology of the submicron-sized WC-13 wt.% Co powder (powder A). Each powder granule is an agglomerated mix of the WC and Co particles. The as-received powder is not very dense as indicated by the pores and voids observed within each granule. The white particles indicated in Figs. 1 (a) and (b) are WC and the gray phase is the cobalt, as determined with the EDS function. Fig. 1 (b) shows that powder A consists mainly of ultrafine WC particles less than 500 nm in size and a few fine WC particles about 1 to 2 μm in size. Most of the ultrafine WC particles have irregular equiaxed shapes and some of the fine WC particles show a typical prism shape [18] (marked with an arrow in Fig. 1 (b)) with well-defined surfaces. The results of the chemical analysis for powder A are listed in Table 2. It can be seen that this powder contains approximately 87 wt.% of WC, 13 wt.% of Co and a small amount of other contaminants. The theoretical density of this powder was calculated to be 14.3 g/cm^3. The XRD spectrum for the as-received powder A is shown in Fig. 2 (a) (spectra for two laser deposited thick wall specimens are also included here for comparison). Five sharp peaks of WC phase and two weak peaks of cobalt were observed. Peaks for the contaminant phases are undetectable due to their low concentrations.
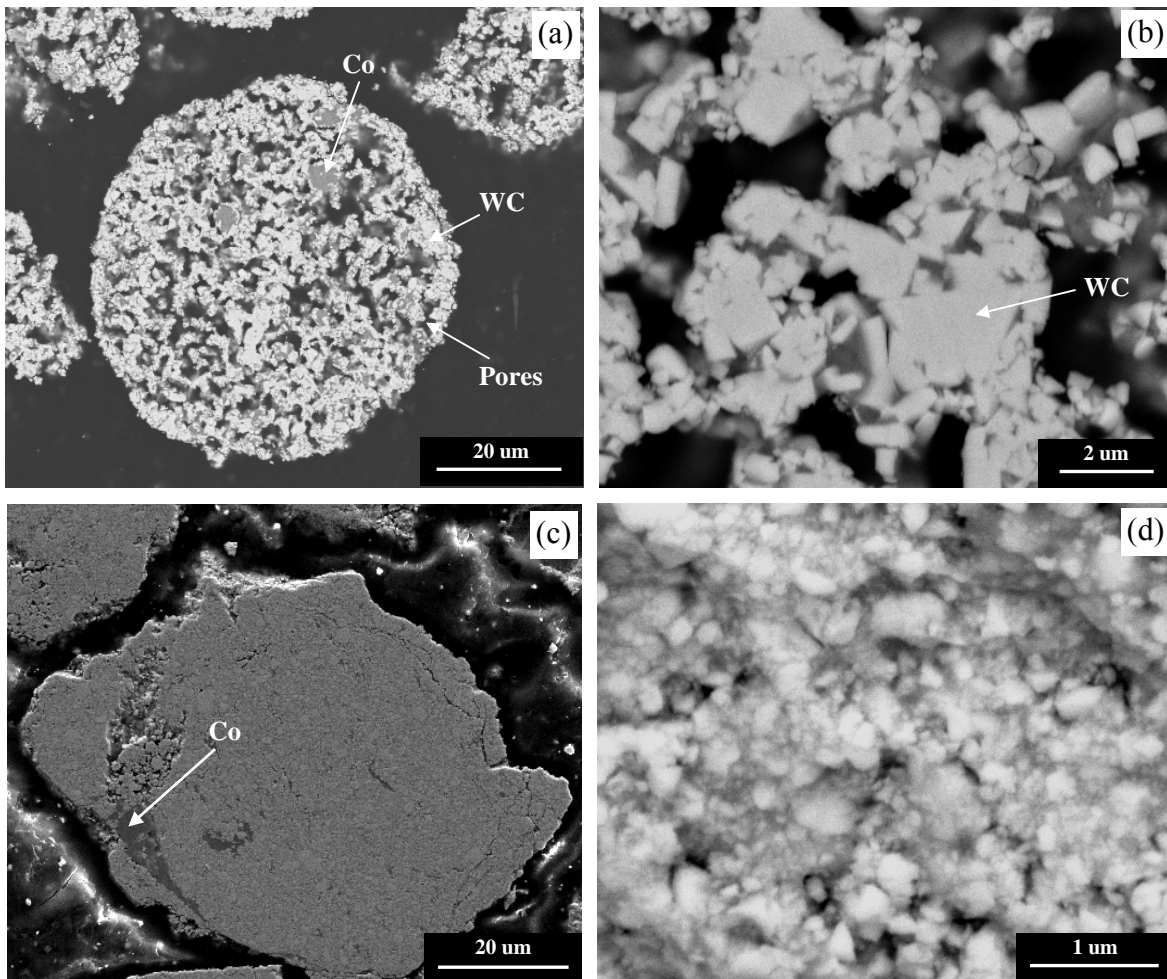

Fig. 1-SEM images of the as-received powders: (a),(b) image of submicron-sized WC-13 wt.% Co powder (powder A); (c), (d) images of nanocrystalline WC-10 wt.% Co powder (powder B).

Table 2. Chemical composition of the as-received powder A and B.

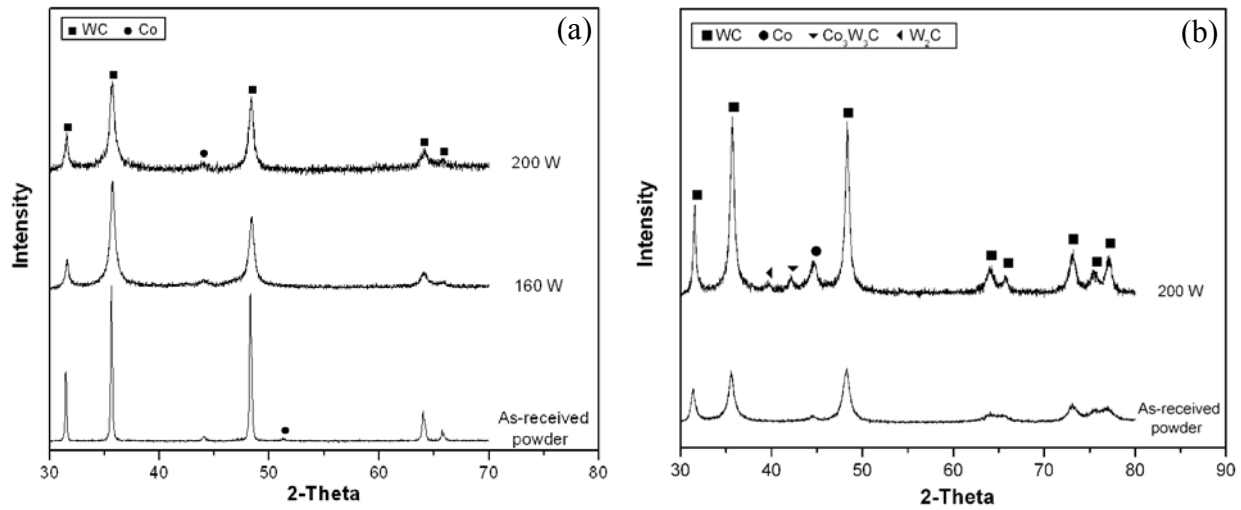| Elements	Weight percentage	
	Powder A	Powder B
W	81.80%	80.00%
C	5.11%	5.05%
Co	12.50%	10.20%
Fe	0.06%	2.98%
Al	0.01%	1.43%
Others	0.52%	0.34%

Fig. 2-XRD spectra for (a) the as-received powder A and two laser deposited specimens; (b) the as-received powder B and one laser deposited specimen.

The SEM images for feedstock powder B are presented in Figs. 1 (c) and (d). It can be seen that this dense nanocrystalline powder has an irregular shape with few pores, which is quite different than powder A (Fig. 1 (a)). Shown in Fig. 1 (d), most of the WC grains are less than 100 nanometers in size and some of them agglomerate to larger particles within the cobalt binder. Most of the WC grains have irregular equiaxed shapes, and do not exhibit a regular prism shape. The results of the chemical analysis for powder B are also listed in Table 2, revealing that powder B contains about 85 wt.% of WC and 10 wt.% of Co. The remaining 5 wt.% is contamination consisting mainly of iron (Fe) and aluminum (Al) generated during the ball milling process. The theoretical density of powder B was calculated to be 13.3 g/cm^3. The XRD spectrum for the as-received nanostructured WC-Co powder is shown in Fig. 2 (b) (the XRD spectrum for one thick wall specimen is also shown here for comparison). Same to powder A, no peaks for the contaminant phases are observed. Therefore, the effect of contaminates are not considered in this paper. Significant peak broadening was found due to the effects of nano-sized grains and micro-strain generated during the ball milling process.

B. Influence of Process Parameters
The effects of laser power, powder feed rate, traverse speed, and working distance on sample microstructure and profile are reported in this section. Powder A was used to study the influence of laser power, powder feed rate, and traverse speed. Due to lack of powder A and its

submicron-sized WC particles, the nanocrystalline WC-10 wt.% Co powder (powder B) was used to study the effect of working distance. It should be noted here that no matter what type of powder is used, the variation of processing parameters should have similar effect on specimens made from the same powder.

I. Influence of Laser Power

Laser power is one of the most important process parameters, which controls specimen microstructure and profile. Specimens studied in this section were made from powder A. The XRD spectra for the deposited specimens at different laser power values (160W and 200W) are shown in Fig. 2 (a). Other processing parameters were held constant for these two specimens: traverse speed was 2.1 mm/s; powder feed rate was 7.0 g/min; layer thickness was set as 0.127 mm and working distance was set with the focal plane of the laser beam. It can be seen that the samples deposited at different laser power levels show similar characteristics as those for the as-received powder A. There is no phase difference due to the change of laser power. It can also be found that peaks of W_2C or Co_3W_3C phases were not observed, indicating that WC decomposition did not occur, or was below detectable limits, under these process conditions. The features of the LENS® technique, high cooling rate, short heating time, and low oxygen concentration, are responsible for these results.

Fig. 3 shows the SEM images of the same thick wall specimen (deposited at 200 W) shown in Fig. 2, in which the layers were deposited along the horizontal direction. As seen in Fig. 3 (a), the upper portion of the deposited specimen was very dense with only a few pores. Layer boundaries cannot be found in this region. Alternating layers (marked with a real layer thickness ΔZ) can be observed only in the bottom portion of the sample with a number of large pores (see Fig. 3 (c)). The pores may result from the pre-existing pores in the as-received powder and lack of enough heat to melt the delivered powder. It should be noted that the real layer thickness ΔZ is about 0.4 mm, which is much larger than the incremental movement of the laser head in the Z direction of, 0.127 mm, between layers. As a consequence, the working distance becomes smaller and smaller, forming a defocusing condition, as the sample is built up. Compared with the images of the as-received powder A, a detailed view of the upper portion of the specimen in Fig. 3 (b) reveals that the size of the WC particles does not change significantly; some of the small particles have either coalesced along their smooth surfaces or just joined together randomly to form one large particle (labeled with an arrow). A magnified image with clear light-dark layer boundaries in the bottom portion is shown in Fig. 3 (d). Most of the WC particles remain ultrafine in particle size in the dark layers. A coalescence phenomenon can be observed throughout the light layers, resulting in the formation of many large WC particles. Remelting of the Co binder in the top portion of the previous layer is responsible for this coalescence phenomenon. Comparison between the microstructural features of the top and bottom portions (Figs. 3 (a) and (c)) indicates that a shorter working distance at a higher working plane is helpful to obtain a uniform microstructure with finer WC particles. This behavior is discussed in further detail in Section B. IV. The density of the bulk specimen shown in Fig. 3 was determined to be 11.7 g/cm³, which is approximately 81% of the theoretical density of powder A. The thick wall specimen deposited at 160 W has a similar microstructure as the one deposited at 200 W except that the layer thickness ΔZ is smaller than 0.4 mm.
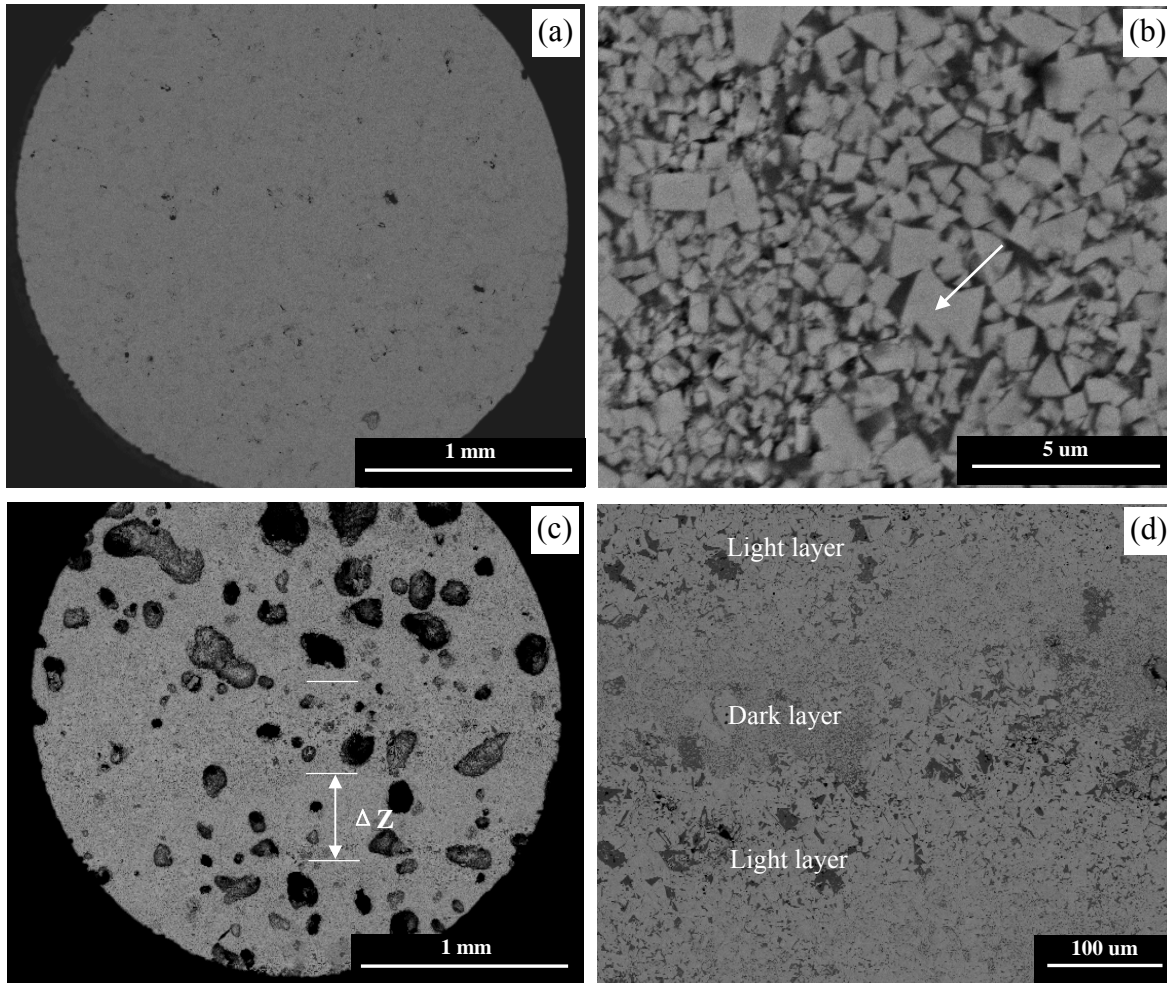
Fig. 3-SEM images of a WC-13 wt.% Co thick wall specimen using powder A deposited at laser power of 200 W and a working plane at the focal plane: (a) upper portion of the specimen; (b) magnified image of (a); (c) bottom portion of the specimen (the white arrows show the 0.4 mm layer thickness of one deposition layer); (d) magnified image of (c) showing clear light-dark layer boundaries.

The influence of laser power on layer thickness is verified by specimen height. As seen in Fig. 4, the specimen height increases with laser power. Here, the height of one specimen deposited at 140 W is also included for comparison. This phenomenon can be explained as follows: with an increase in laser power, the temperature of the molten pool increases; the width and height of the molten pool also increase, resulting from more powder included in each molten pool. The layer thickness is also controlled by the increment in Z height set by the operator. If the height of the molten pool is close to but greater than the set Z height increment, the part builds with layer thickness equal to the Z height increment. Only the top layer will have the height of the molten pool resulting in a slight increase in final height. If the height of the molten pool is much greater than the set Z height increment, the part builds initially with a layer thickness higher than the Z height increment, which could later cause the focus point of the laser beam to be below the top of the part being built, a defocus situation of the laser beam. Laser power achieved in the heat affected zone would then be reduced and less powder would be deposited onto the previous layer. Consequently, layer thickness may become much smaller or

no layer boundaries will occur in the upper portion of the specimen. Because of the lower laser power, particle coarsening or coalescence is limited. This condition will continue until the distance between the top of the specimen and the focus point is close to zero. This might be the reason why, in Fig. 3, the observed layer thickness (about 0.4 mm) in the bottom portion is much higher than the set value (0.127 mm); however, the upper portion is relatively dense and smooth without layer boundaries. Because the set specimen height in the CAD solid model used in this study is not high enough to compensate for the height difference, the final specimen height increases with laser power due to the increase of layer thickness in specimen's bottom portion.
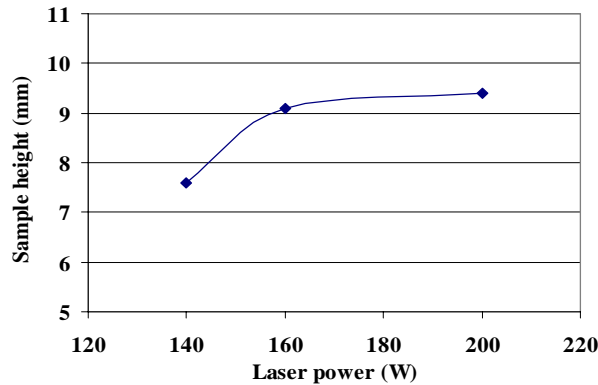

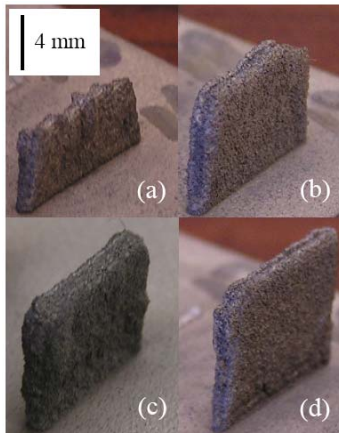Fig. 4-The influence of laser power on sample height.

Fig. 5-The influence of powder feed rate on sample profile: (a) 11.0 g/min; (b) 12.4 g/min; (c) 14.9 g/min; (d) 20.4 g/min.
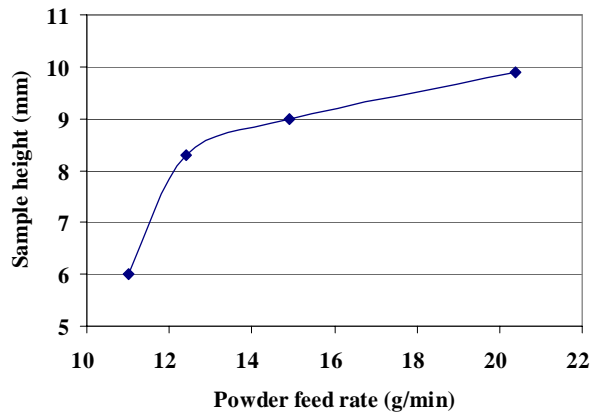

Fig. 6-The influence of powder feed rate on sample height.

II. Influence of Powder Feed Rate

Powder feed rate is a process parameter that is used to control the amount of powder fed into the focal point of the laser beam per unit time. Laser deposited specimens studied in this section were made from powder A. The effects of powder feed rate on specimen profile and height are shown in Figs. 5 and 6. Other processing parameters were held constant for these four specimens: laser power was 160 W; traverse speed was 6.4 mm/s; layer thickness was set as 0.127 mm and working plane was set at the focal plane of the lens. From these results, it can be seen that powder feed rate has a significant impact on a specimen's shape and height. At lower powder feed rate (Fig. 5 (a)), less powder than required is heated by the laser beam. The molten pool is relatively small and the actual layer thickness is smaller than the desired value as a result. Since

the increment of movement for the laser head for each layer is set equal to the desired layer thickness, the working distance increases resulting in an over-focus condition of the laser beam. In this case, the laser intensity is lower and part of the delivered powder is not melted completely, leaving some porosity. If the powder feed rate is too low, the top of the previous layer will be too low to deposit any new powder on its surface. Thus, building stops. The final height is then much smaller than expected.

III. Influence of Traverse Speed

Traverse speed is another critical process parameter that controls the speed of the moving substrate. Powder A was used as the starting powder for the deposited specimens studied in this section. Figs. 7 and 8 show the effects of traverse speed on specimen profile and height. Other processing parameters were held constant for the three specimens: laser power was 160 W; powder feed rate was 14.9 g/min; layer thickness was set as 0.127 mm and working plane was set at the focal plane of the lens. It can be seen that when traverse speed is too high (Fig. 7 (c)), the specimen profile is unacceptable; building stops due to a working distance much larger than the desired value. High traverse speed can cause insufficient powder per unit length. Thus, less powder than required is remelted by the laser beam. This indicates that at constant laser power and working distance, high traverse speed can have a similar effect as that of low powder feed rate.
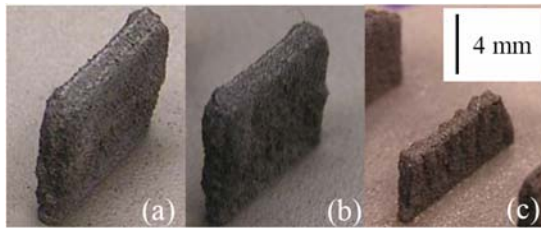
Fig. 7-The influence of traverse speed on sample profile: (a) 4.2 mm/s; (b) 6.4 mm/s; (c) 10.6 mm/s.
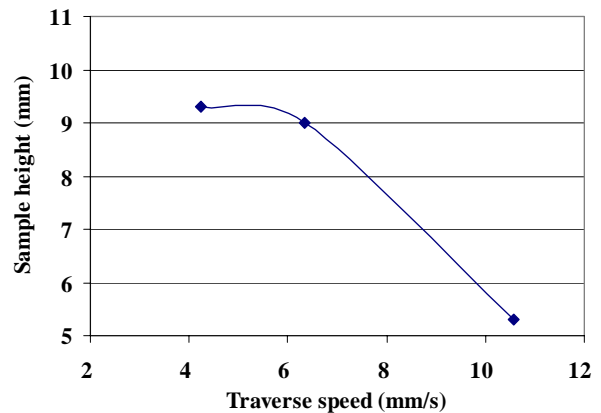
Fig. 8-The influence of traverse speed on sample height.

IV. Influence of Working Distance and Relative Location of the Focal Plane

Process conditions, such as laser power, powder feed rate and traverse speed are significant parameters that are generally optimized in order to enhance material properties. The working distance is selected by the operator, and fixed during the LENS® process. However, in our study, it was found that variations in working distance play a very important role in microstructure improvement, especially for cermet materials. In this section, the effect of working distance and relative location of the focal plane to the deposition surface was studied based on specimens made from powder B.

Dense thick wall specimens were produced by choosing proper deposition parameters. Alternating layers can be observed in the microstructure (see Figs. 9 (a) and (b)). The laser power was 200W; traverse speed was 3 mm/s; and powder feed rate was 10 g/min. Layer thickness was set as 0.203 mm. The working plane was 2 mm higher than the focal plane of the lens. For Fig. 9 (a), layers were deposited along the horizontal direction and for Fig. 9 (b), layers

were deposited along the direction perpendicular to the paper. The observed layer thickness (about 0.2 mm, marked with ΔZ) matched well with the set value, 0.203 mm. It can be seen that the areas with alternating layers shown in both Figs. 9 (a) and (b) are much denser than the ones presented in Fig. 3 (c) with pores due to lack of fusion and pre-existing pores in the as-received powder. The density of the bulk specimen shown in Fig. 9 was tested and calculated to be 12.9 g/cm^3, which is approximately 97% of the theoretical density of powder B. The calculated relative density is much higher than other published reports in the field of bulk WC-Co production using laser-related techniques [19]. Dense feedstock powder and proper selection of process parameters contribute to the density improvement. In Fig. 9 (c), not only the white phase WC and black phase Co can be found, but also the gray phase Co_3W_3C can occasionally be observed, as determined by EDS. This observation is also verified by the XRD result shown in Fig. 2 (b) for the laser deposited sample. The W_2C phase is not observed in the SEM images due to its low concentration. Although the heating/cooling rate for the LENS® process is high, the feedstock powder contains nanostructured WC grains that have high surface area per unit volume, resulting in a great likelihood of being dissolved into the liquid phase at high temperature [20]. Furthermore, the powder does not have free carbon to compensate for any carbon loss that might occur during the process. Thus, it is possible to find a small amount of Co_3W_3C phase after deposition. It is observed that grain growth is limited to a certain extent during laser deposition. Some grains remain in a size less than 100 nm. Some grow to a size in the submicron or micron regimes. Previous work reported that the large white particles are not WC single crystals, but polycrystals containing WC grains with a size ranging from tens of nanometers to one or two microns [21].
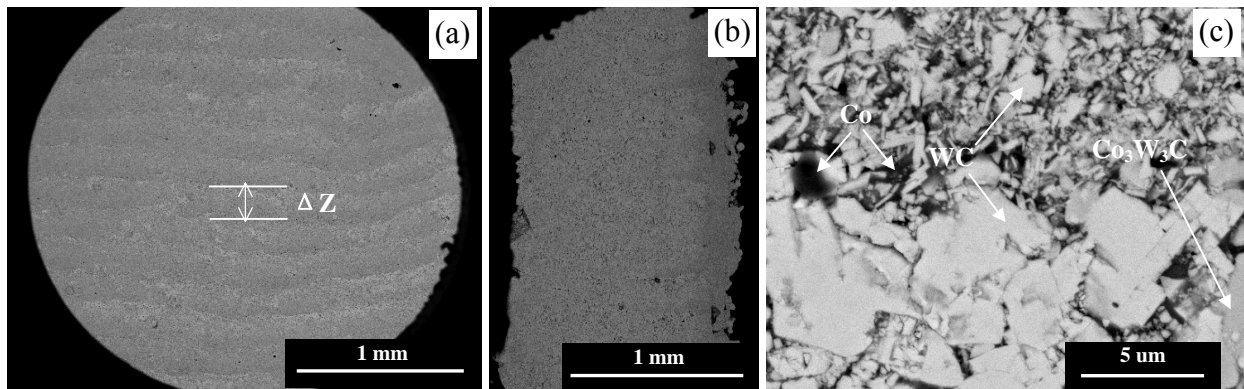

Fig. 9-SEM images of a WC-10 wt.% Co thick wall specimen deposited with powder B at laser power of 200 W and a working plane 2 mm higher than the focal plane: (a) image at low magnification showing alternating layers (the white arrows show the 0.2 mm layer thickness of one deposition layer); (b) cross-sectional image at low magnification; (c) enlarged image of (a) showing a boundary area between the alternating layers with fine WC particles in the dark layer and large WC particles in the light layer.

Fig. 10 contains SEM images of a deposited specimen using similar process parameters to the one demonstrated in Fig. 9. Two changes were made: the working plane was about 4 mm higher than the focal plane of the lens; and the layer thickness was set as 0.127 mm. Uniform microstructure without layer boundaries throughout the whole sample area was observed. Even more, particle coarsening was not significant, as shown in Fig. 10 (b), which is believed to be related to the unique thermal behavior: a shorter working distance at a higher working plane resulting in lower laser intensity. This is discussed in more detail in the following paragraphs.

The X-ray spectrum of this specimen is not shown here. There is no phase difference between this specimen and the one shown in Fig. 9 deposited with a longer working distance. The density of this bulk specimen (shown in Fig. 10) was 12.8 g/cm^3 (96% of the theoretical density), which is comparable to the density of the other bulk specimen (shown in Fig. 9).
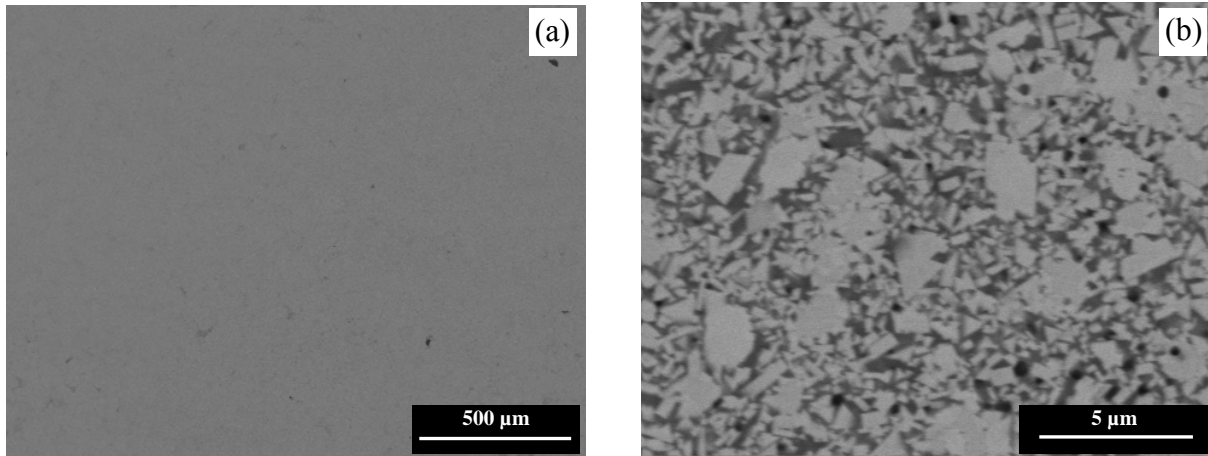

Fig. 10-SEM images of a WC-10 wt.% Co thick wall specimen deposited with powder B at laser power of 200 W and a working plane 4 mm higher than the focal plane: (a) image at low magnification showing uniform microstructure without layer boundaries; (b) image at high magnification showing fine WC particles.
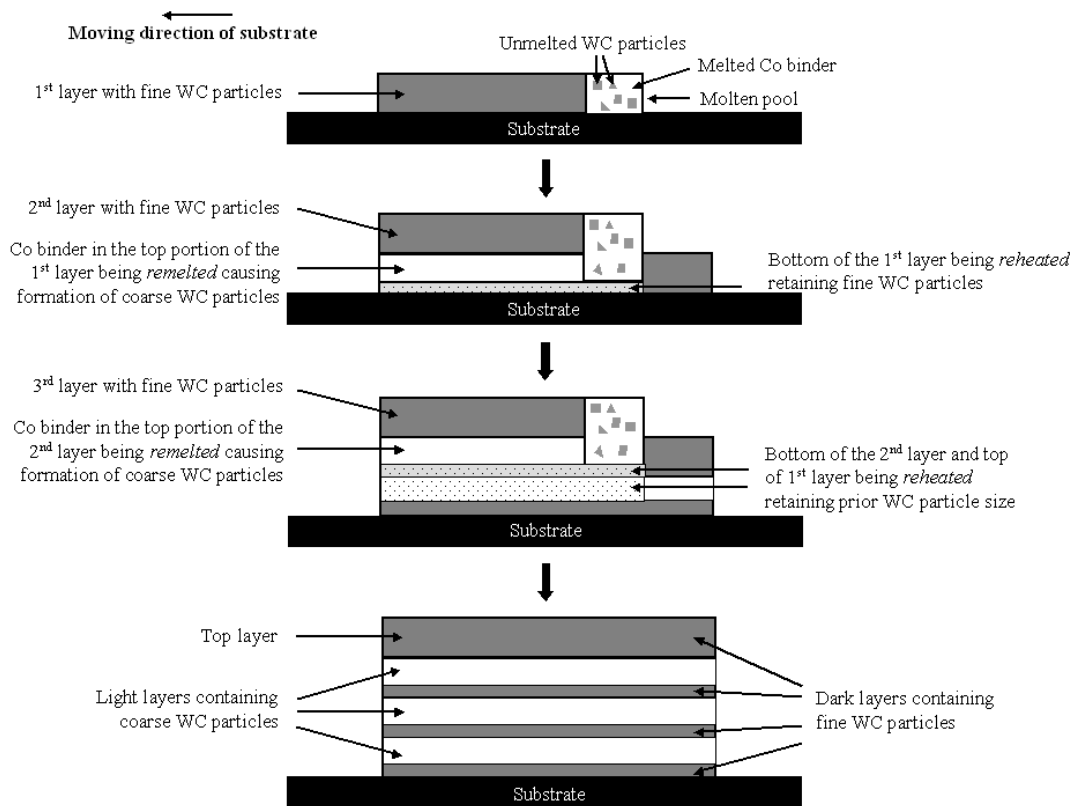

Fig. 11 -A schematic diagram showing the formation of a microstructure with alternating layers deposited with a working distance at the focal plane of the laser beam, matched with a Z height increment equal to the deposit height.

Fig. 11 shows a deposition condition when the working plane is set at the focal plane of the laser beam and other parameters are properly set to ensure the desired layer thickness. When one layer is being deposited, the Co binder in the top portion of the previous layer will be remelted resulting in the coarsening of WC particles in the light layers. However, the bottom portion of the previous layer will only be reheated, retaining the fine WC particles in the dark layers. As specimens are built up, microstructures with alternating layers are generated. As mentioned above, a shorter working distance can result in lower laser intensity. The molten pool then is shorter and the layer thickness is smaller than that for when deposition occurs at the focal plane of the laser beam. Remelting of the Co binder in the top portion of the previous layer can still take place when the working plane is not much higher than the focal plane. Thus, the microstructure with alternating layers will also appear as demonstrated in Fig. 9 (a). To some extent, when the working plane is much higher than the focal plane, the microstructures with alternating layers disappear. Due to the resulting low laser intensity, the effect of remelting is not significant. Reheating of the entire fine particles for a few previous layers would occur instead, forming a larger heat affected zone. Therefore, a smooth microstructure without much grain coarsening is produced, like the one shown in Fig. 10 (a).

V. Optimization of Process Parameters

According to the above analysis on the influence of process parameters for WC-Co cermet fabrication, the preferred ranges for the process parameters during LENS® deposition are summarized in Table 3. With a constant initial setting for working distance, the variations in laser power, powder feed rate and traverse speed determine whether the feedstock powder gains enough heat, per unit powder mass or per unit length along the traverse direction, to create a molten pool. The height of the molten pool affects the actual layer thickness of the building part. The Z height increment should be set equal to the actual layer thickness to maintain the constant working distance. With proper selection of laser power, powder feed rate, traverse speed and Z height increment, the initial setting of working distance will then affect the uniformity of the microstructure. The application of a shorter working distance leads to improvement in specimen density and microstructure.

Table 3. Preferred range of process parameters for WC-Co cermets by the LENS®.

Experimental Parameter	Range
Laser power	180-200 W
Powder feed rate	7-10 g/min
Traverse speed	2-4 mm/s
Working plane	Focal plane + 2~4 mm

Conclusions

WC-Co thick wall specimens were produced using submicron-sized WC-13 wt.% Co powder and nanostructured WC-10 wt.% Co powder by the LENS® process. The results of this study are summarized as follows. Decomposition of WC is sensitive to grain size. Decomposition did not occur when submicron-sized powder was used, which results from the high cooling rate, short heating time and low oxygen concentration during the LENS® process. However, it occurred when nano-sized powder was used. Microstructures both with or without alternating layers can be fabricated by controlling key process parameters. Particle coarsening was not significant in the specimens with a homogeneous microstructure. Processing conditions,

such as laser power, powder feed rate, traverse speed, and working distance have significant effects on the profiles and microstructures of the deposited thick walls. Sample height increases with the increase of laser power, powder feed rate or the decrease of traverse speed. The application of a shorter working distance leads to improvement in specimen density and microstructure.

Acknowledgements

References

[1] A. Parasiris, K. T. Hartwig, International Journal of Refractory Metals & Hard Materials 18 (2000) 23-31.
[2] P. Seegopaul, L. E. McCandlish, F. M. Shinneman, International Journal of Refractory Metals & Hard Materials 15 (1997) 133-138.
[3] X. M. Ma, G. Ji, Journal of Alloys and Compounds 245 (1996) L30-32.
[4] B. H. Kear, L. E. McCandlish, Nanostructured Materials 3 (1993) 19-30.
[5] L. E. McCandlish, B. H. Kear, B. K. Kim, Nanostructured Materials 1 (1992) 119-124.
[6] C.-C. Jia, H. Tang, X.-Z. Mei, F.-Z. Yin, X.-H. Qu, Materials Letters 59 (2005) 2566–2569.
[7] D. Sivaprahasam, S. B. Chandrasekar, R. Sundaresan, International Journal of Refractory Metals & Hard Materials 25 (2007) 144-152.
[8] Y. Zhu, C. Ding, K. Yukimura, T. D. Xiao, P. R. Strutt, Ceramics International 27 (2001) 669-674.
[9] R. W. Smith, R. Knight, JOM 47 (1995) 32-39.
[10] V. V. Sobolev, J. M. Guilemany, International Materials Reviews 41 (1996) 13-32.
[11] D. M. Keicher, J. L. Jellison, L. P. Schanwald, J. A. Romero, D. H. Abbott, Towards a reliable laser spray deposition system through process characterization, in: Proceedings of the 27th international technical conference of the Society for the Advancement of Material and Process Engineering (SAMPE), vol 27, Albuquerque, New Mexico, 1995, pp. 1029-1039.
[12] W. Hofmeister, M. Griffith, M. Ensz, J. Smugeresky, JOM 53 (2001) 30-34.
[13] M. L. Griffith, M. T. Ensz, J. D. Puskar, C. V. Robino, J. A. Brooks, J. A. Philliber, J. E. Smugeresky, W. H. Hofmeister, Understanding the Microstructure and Properties of Components Fabricated by Laser Engineered Net Shaping (LENS®), in: Proceedings of solid freeform and additive fabrication-Materials Research Society Symposium, vol 625, San Francisco, CA, USA, 2000, pp. 9-20.
[14] W. Liu, J. N. DuPont, Scripta Materialia 48 (2003) 1337-1342.
[15] G. K. Lewis, E. Schlienger, Materials and Design 21 (2000) 417-423.
[16] W. Liu, J. N. Dupont, Metallurgical and materials transaction A 35A (2004) 1133-1140.
[17] C. L. Atwood, M. Griffith, L. Harwell, E. Schlienger, M. Ensz, J. E. Smugeresky, T. Romero, D. Greene, D. Reckaway, Laser engineered net shaping (LENS®): a tool for direct fabrication of metal parts, in: Proceedings of ICALEO '98, vol 85, Orlando, FL, USA, 1998, pp. E-1.
[18] T. Yamamoto, Y. Ikuhara, T. Sakuma, Science and Technology of Advanced Materials 1 (2000) 97-104.
[19] T. Glaeser, F. Klocke, T. Bergs, Liquid phase sintering of tungsten carbide with both cobalt and nickel binder phases by laser radiation, in: Proceedings of the Sixth International Conference on Tungsten, Refractory & Hardmetals, Orlando, FL, USA, 2006, pp. 132-139.
[20] J. He, J. M. Schoenung, Surface and Coatings Technology 157 (2002) 72–79.
[21] Y. Xiong, J. E. Smugeresky, L. Ajdelsztajn, J. M. Schoenung, Materials Science and Engineering A (2008) in press.